Evolution of the optical properties of alkali-metal microclusters towards the bulk: The matrix random-phase approximation description

C. Yannouleas* and E. Vigezzi
Istituto Nazionale di Fisica Nucleare, Sezione di Milano, Via Celoria 16, I-20133 Milano, Italy

R. A. Broglia
Dipartimento di Fisica, Università di Milano, and Istituto Nazionale di Fisica Nucleare, Sezione di Milano, Via Celoria 16, I-20133 Milano, Italy
and The Niels Bohr Institute, University of Copenhagen, DK-2100 Copenhagen Ø, Denmark
(Received 19 June 1992; revised manuscript received 22 October 1992)

The evolution toward the bulk values of the energy centroid and of the width characterizing the surface-plasmon resonance in spherical neutral sodium clusters is studied. For this purpose, the photoabsorption spectrum of clusters comprising from 8 to 338 atoms is calculated microscopically making use of the jellium shell model to describe the motion of delocalized electrons and of the matrix random-phase approximation to determine the collective response of the system to electromagnetic radiation. The Coulomb force is treated in the local-density approximation. The case of large potassium clusters having approximately 500 and 900 atoms is also considered.

I. INTRODUCTION

It is well known that a shell-model picture applies to both elemental atoms and atomic nuclei, despite the differences in the forces involved. This is also the case for a variety of metal clusters, that is, aggregates containing a small number of atoms. Indeed, one can assume that the valence electrons in a metal cluster, such as sodium, are delocalized and explore the total volume of the cluster, their motion being prescribed by a central average field, as is the case of atomic nuclei. In the case of the alkali metals, a reasonable approximation to the average shell-model field is provided by invoking the jellium model,[1] based on the fact that the detailed positions of the ions do not play an important role. Rather, one can replace the ionic lattice with a uniform, positively charged background.

Aside from the static (ground-state) properties of small metal clusters (cf., e.g., Ref. 1 and references therein), the dynamical response of the system to external probes has recently received attention. In particular, it has been observed that metal clusters can absorb light through the excitation of a collective mode produced by the motion of electrons against the positive ionic background. This surface plasmon has been known from experiments in very large clusters,[2] but it is only in the last few years that it has been observed in the region of low mass numbers.[3–8]

For the description of the surface plasmon in large clusters, the classical Mie theory[9] has provided a useful framework. According to this theory, there is one single surface-plasmon peak carrying 100% of the oscillator strength at the energy

$$\hbar\omega_p/\sqrt{3}\ , \tag{1}$$

where

$$\hbar\omega_p = \sqrt{4\pi\rho e^2/m_e} \tag{2}$$

is the energy of the volume plasmon in the bulk metal (ρ is the electronic density and m_e is the free-electron mass). Experimentally, the width of this resonance has been found to be Av_F/R, where v_F is the Fermi velocity of the conduction electrons, R is the radius of the cluster, and A is a proportionality constant of order unity.[2] Theoretical approaches, based on an analytical treatment of linear-response[10] and random-phase-approximation[11,12] (RPA) methods in the limiting case of a large volume have reproduced this $1/R$ dependence.[13] The physics underlying this smooth dependence is that of Landau damping[14] as modified for the case of a finite, but large, system with quasicontinuum single-particle spectra.

For clusters of low mass ($\leq$ 40 atoms), this classical picture was also applied in an attempt to interpret the observation.[3,4] However, systematic measurements[5] of the photoabsorption cross section on free sodium clusters in this mass region have revealed a much more complicated and nontrivial line shape (cf. also Refs 7 and 8). In particular, a high degree of fragmentation in several peaks is present. In addition, the $1/R$ law for the broadening of these peaks breaks down, as noticed in Ref. 6. Instead, a broadening process due to the fluctuations of the surface of the cluster[15–19] seems to be able to account for the observed widths.

The fragmentation of the photoabsorption strength in several distinct peaks was explained as a quantum-size effect in terms of an especially strong coupling between the surface plasmon and the highly discretized single-particle motion (a special realization of Landau damping reflecting the discreteness of the single-particle spectra), and is manifested in numerical RPA (Refs. 20, 17, and 21) or TDLDA (Refs. 22–25) (time-dependent local-density-

approximation) calculations [cf. especially the cases of Na_8, Na_{20}, and Na_{40} (Refs. 20, 21, and 26)].

In this paper we describe the evolution with size of the optical properties of alkali-metal clusters from the very small to the very large. In this respect, the present study helps to bridge the gap in our knowledge from the atom to the bulk, an objective that is central in cluster research. As mentioned earlier, optical measurements on both ends of this gap—namely, on very large silver clusters embedded in a host medium,[2] and on very small alkali-metal clusters[3–8]—have been available in the last few years. However, the intermediate cluster sizes have been much less studied, both experimentally and theoretically. In particular, we are unaware of any theoretical study that has attempted to provide a global picture for the evolution of the optical response by accounting simultaneously for the behavior of both the profile and the position of the photoabsorption cross sections. Developing such a picture is the aim of the present work.

Specifically, we extend previous matrix RPA calculations[20,21] for the neutral sodium clusters to higher magic numbers, up to 338. We are thus able to study the systematics of the evolution of the optical response with the size of the cluster, and its approach towards the bulk. This subject is of significant interest also in view of the fact that optical measurements on larger sodium (up to 300) (Ref. 27) and potassium clusters[28] (K^+_{500} and K^+_{900}) have been recently reported.

In particular, we find that the peak of the surface plasmon in sodium, although starting with a 20% lower value in the case of Na_8, converges rather rapidly to the classical Mie value, $\hbar\omega_p/\sqrt{3}$, as was recently observed experimentally.[27] Special attention is given to the evolution of the Landau fragmentation in several peaks, and the transition to the regime of the $1/R$ law. The evolution of the polarizability is also studied. Conclusions are drawn on the improving applicability of the jellium approximation with increasing size of the sodium clusters, at least with respect to the description of optical properties.

In the case of potassium clusters, we found that—contrary to the case of sodium clusters where the RPA-LDA is able to provide an accurate description of the data—theory deviates significantly from experiment.[28] Indeed, the peak of the photoresonance in potassium clusters converges to a value considerably lower than the Mie value given by Eq. (1). We suggest that this discrepancy is due to the free-electron-gas parameters used until now as input in the RPA equations. Consideration of an effective mass, as well as of core-polarization contributions, deduced from the bulk optical response for potassium can bring the RPA-LDA results in overall agreement with experiment.

Compared to a molecular *ab initio* treatment, the present matrix RPA-LDA upon a jellium background constitutes a rather simple approach. In this respect, it is encouraging that this approach is flexible enough to yield satisfactory results for the full range of cluster sizes, from the very small to the very large—especially, since the molecular calculations are restricted to small sizes (below 20 atoms).[29] Since the matrix RPA formalism has only partially been discussed in previous publications,[20,21] we provide here a complete exposition.[30] This is especially desirable, in view of the fact that this formalism is known in nuclear physics in a different angular-momentum coupled scheme, namely the j-j scheme, unlike the present LS coupling scheme, appropriate for metal clusters.

The plan of this paper is as follows. Section II offers a concise theoretical exposition of the discrete-matrix RPA formalism as applied to spherical metal clusters. Section III presents the general trends in the results of the matrix RPA calculations for sodium and compares them with the experimental data. Section IV discusses the corresponding calculations for large potassium clusters. Finally, Sec. V provides a summary and conclusions.

II. DISCRETE MATRIX RPA FOR SPHERICAL CLUSTERS

A. The matrix equations

The spherical shape of metal clusters associated with a magic number allows for a significant computational simplification of the discrete matrix RPA equations.[31] In this case, since the angular momentum is a good quantum number, one can sum algebraically over its projections and eliminate them from the RPA equations, drastically reducing in the process the size of the matrices to be diagonalized. To this effect, one introduces an angular-momentum coupled creation operator $A^\dagger_{ph}(L,M)$ (Ref. 32) as a linear superposition of uncoupled particle-hole operators $a^\dagger_p a_h$, having angular momenta l_p and l_h, namely,

$$A^\dagger_{ph}(L,M)=\frac{1}{\sqrt{2}}\sum_{m_p,m_h,\sigma}(l_p,l_h,m_p,m_h|LM)(-)^{l_h+m_h}\times a^\dagger_{l_p,m_p,\sigma}a_{l_h,-m_h,\sigma}\ , \tag{3}$$

where the index σ denotes the spin variable. The operator $A^\dagger_{ph}(L,M)$, as written in Eq. (3), represents a singlet spin state ($S=0$) and the $1/\sqrt{2}$ factor imposes the normalization condition in the spin space. That the RPA state is singlet in spin follows from the fact that the Coulomb force is central and thus cannot flip the spin of the excited particles. The expression in parentheses is the usual Clebsch-Gordan coefficient[33] expressing the coupling of two angular momenta (l_1,l_2) with projections (m_1,m_2) to a total angular momentum L with total projection M. Observe that here we work in the LS coupling scheme, unlike the j-j scheme familiar from nuclear physics.[31] The reason is that the spin-orbit terms in metal clusters can be neglected, unlike the case of atomic nuclei.

With the coupled operators $A^\dagger_{ph}(L,M)$, the RPA phonon-creation operator $O^\dagger_\nu(L,M)$ is written as follows:

$$O^\dagger_\nu(L,M)=\sum_{ph}\{X^\nu_{ph}(L)A^\dagger_{ph}(L,M)-(-)^{L+M}Y^\nu_{ph}(L)A_{ph}(L,-M)\}\ . \tag{4}$$

Examples of the coupled particle-hole transitions $A^{\dagger}_{ph}(L,M)$ entering into Eq. (4) are displayed in Fig. 1.

Then the full RPA equation reduces to a set of identical submatrix equations, each specified by a given total angular momentum $L=\lambda$, where λ is the multipolarity of the plasmon. In particular, these submatrix equations are

$$\begin{pmatrix} A^{\lambda} & B^{\lambda} \\ -B^{\lambda *} & -A^{\lambda *} \end{pmatrix} \begin{pmatrix} X^{\nu} \\ Y^{\nu} \end{pmatrix} = E_{\nu} \begin{pmatrix} X^{\nu} \\ Y^{\nu} \end{pmatrix} , \tag{5}$$

where the elements of the A^{λ} and B^{λ} are specified by the double commutators,

$$A^{\lambda}(ph,p'h') = [A_{ph}(\lambda,\mu),[H,A^{\dagger}_{p'h'}(\lambda,\mu)]] \tag{6}$$

and

$$B^{\lambda}(ph,p'h') = (-)^{\lambda+\mu+1}[A_{ph}(\lambda,\mu),[H,A_{p'h'}(\lambda,-\mu)]] . \tag{7}$$

In Eqs. (6) and (7), H is the many-body Hamiltonian; it consists of two parts, a static single-particle part H_0 and the residual two-body interaction V,

$$H = H_0 + V . \tag{8}$$

The static part H_0 is the sum of the kinetic energy T of the free conduction electrons plus the average potential $U(r)$ that binds them in the cluster, namely,

$$H_0 = \sum_{i}^{N_e} \{T_i + U_i(r)\} . \tag{9}$$

In what follows, we shall specify the single-particle potentials self-consistently in the spherical jellium-background model[22] using the density-variational formalism in a semiclassical approximation.[34] As an example, the potential for Na_{58} is displayed in Fig. 1.

The residual two-body interaction V is taken according to the local-density approximation to be

$$V(\mathbf{r}_1,\mathbf{r}_2) = \frac{e^2}{|\mathbf{r}_1-\mathbf{r}_2|} + \frac{dV_{\rm xc}[\rho]}{d\rho}\ \delta(\mathbf{r}_1-\mathbf{r}_2) . \tag{10}$$

Here $V_{\rm xc}[\rho] = d\mathcal{E}_{\rm xc}[\rho]/d\rho$ is the exchange-correlation potential in the ground state. As in Refs. 22 and 34, we use the exchange-correlation energy density $\mathcal{E}_{\rm xc}[\rho]$ of Gunnarsson and Lundqvist.[35] As a result, the exchange-correlation potential $V_{\rm xc}$ is given in atomic units (energy in Ry) by the expression

$$V_{\rm xc}(\mathbf{r}) = -1.222/r_s(\mathbf{r}) - 0.0666 \ln\left(1+\frac{11.4}{r_s(\mathbf{r})}\right) , \tag{11}$$

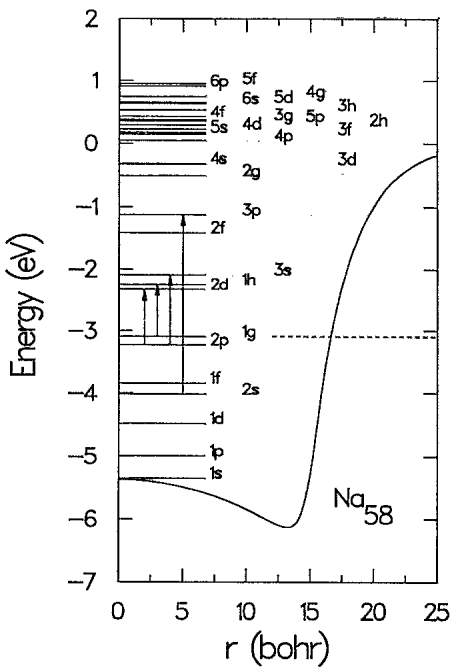

FIG. 1. Jellium potential associated with Na_{58}. The ensuing single-particle levels relevant to the excitation of the dipole resonance, as well as some of the associated unperturbed particle-hole transitions (vertical arrows), are also shown. The horizontal dashed line indicates the highest filled single-particle level.

where $r_s(\mathbf{r}) = [3/4\pi\rho(\mathbf{r})]^{1/3}$ is the local value of the Wigner-Seitz radius. The values of the parameters entering into Eq. (11) were obtained in Ref. 35 by adjusting the correlation functional to the results of the RPA correlations computed in a homogeneous electron gas.

To calculate the double commutators in Eqs. (6) and (7) defining the RPA matrices in the coupled representation, one needs the corresponding RPA result in the case of the uncoupled representation, namely, that

$$[a^{\dagger}_h a_p,[H,a^{\dagger}_{p'}a_{h'}]]_{\rm RP} = (\epsilon_p-\epsilon_h)\delta_{pp'}\delta_{hh'} + V_{ph'hp'} \tag{12}$$

and

$$-[a^{\dagger}_h a_p,[H,a^{\dagger}_{h'}a_{p'}]]_{\rm RP} = V_{pp'hh'} . \tag{13}$$

Then a direct calculation of the double commutators (6) and (7) allows for an explicit integration over the angles and summation over the angular-momentum projections. The result for the elements of the RPA matrices in the coupled representation is

$$\begin{aligned} &A^{\lambda}(ph,p'h') - (\epsilon_{n_p,l_p}-\epsilon_{n_h,l_h})\delta_{l_p,l_{p'}}\delta_{l_h,l_{h'}}\delta_{n_p,n_{p'}}\delta_{n_h,n_{h'}} \\ &= 2R^{\lambda}(ph',hp')(-)^{l_p+l_{p'}}\frac{[(2l_p+1)(2l_h+1)(2l_{p'}+1)(2l_{h'}+1)]^{1/2}}{(2\lambda+1)} \begin{pmatrix} l_h & \lambda & l_p \\ 0 & 0 & 0 \end{pmatrix} \begin{pmatrix} l_{h'} & \lambda & l_{p'} \\ 0 & 0 & 0 \end{pmatrix} \\ &= (-)^{\lambda}\, B^{\lambda}(ph,p'h') , \end{aligned} \tag{14}$$

where the radial part is of the form

$$R^{\lambda}(ph',hp') = \int r_1^2 dr_1 r_2^2 dr_2 \mathcal{R}_{n_p,l_p}(r_1)\mathcal{R}_{n_{h'},l_{h'}}(r_2)V(r_1,r_2;\lambda)\mathcal{R}_{n_h,l_h}(r_1)\mathcal{R}_{n_{p'},l_{p'}}(r_2)\ . \tag{15}$$

The quantities ϵ_{n_i,l_i} are the single-particle energies specified by the static Hamiltonian H_0, while $\mathcal{R}_{n_i,l_i}(r)$ is the radial part of the single-particle wave functions, the total wave function being $\mathcal{R}_{n_i,l_i}(r)\,\mathcal{Y}_{l_i,m_i}(\theta,\phi)$, with $\mathcal{Y}$ denoting a spherical harmonic. The radial contribution of the two-body interaction (10) in multipole order λ is given by

$$V(r_1,r_2;\lambda) = e^2\,\frac{r_<^{\lambda}}{r_>^{\lambda+1}} + \frac{dV_{\rm xc}[\rho]}{d\rho}\,\frac{\delta(r_1-r_2)}{r_1^2}\,\frac{2\lambda+1}{4\pi}\ , \tag{16}$$

where $r_< = \min(r_1,r_2)$ and $r_> = \max(r_1,r_2)$.

The indices n_i appearing in Eqs. (14) and (15) denote the number of nodes for the corresponding single-particle states. The orbital angular momenta of the particles and holes participating in the excitations are denoted by l_i, the total angular momentum of the excitation being λ, which in the present calculation is set equal to 1 (dipole vibration). The $3j$ symbols appearing in (14) take proper care of the angular-momentum coupling, as well as of the parity-conservation conditions. The factor 2 accounts for the spin degeneracy.

For smaller sizes, the radial wave functions $\mathcal{R}_{n_i,l_i}(r)$ are calculated by diagonalizing the single-particle Hamiltonian H_0 in a basis including 25 harmonic-oscillator major shells. The optimal oscillator parameter of this basis is adjusted to reflect the volume of the cluster. This procedure amounts to a discretization of the continuum. For clusters having more than 300 atoms, we carry the discretization by confining the cluster inside a cavity of large but finite radius. The results are, however, independent of these choices.

It should be noticed [cf. Eqs. (14) and (15)] that the RPA matrices A^{λ} and B^{λ} are real for the special case of the Coulomb interaction. As a result, the RPA amplitudes $X(\lambda)$ and $Y(\lambda)$ are also real. However, for the purpose of generality, we will continue treating them in the notation as if they were complex.

The forward- and backward-going RPA amplitudes $X_{ph}^{\nu}(L)$ and $Y_{ph}^{\nu}(L)$ obey the following orthonormalization condition:

$$\sum_{ph}\{X_{ph}^{\kappa *}(L)X_{ph}^{\nu}(L) - Y_{ph}^{\kappa *}(L)Y_{ph}^{\nu}(L)\} = \delta_{\kappa\nu}, \quad E_{\nu}\geq 0\ . \tag{17}$$

B. The energy-weighted sum rule

An important property of the RPA is that the transition probabilities of a one-body operator between the ground state and the RPA excited states obey several sum rules, and in particular the energy-weighted sum rule (EWSR), which is known as the Thomas-Reiche-Kuhn (TRK) sum rule in the dipole case. In the coupled representation, the transition probability, $B(E\lambda,0\rightarrow\nu)$, associated with the RPA state $|\nu\rangle$ of Eq. (4) can be written as

$$B(E\lambda,0\rightarrow\nu) = \frac{2}{2\lambda+1}\,|\langle\nu||\mathcal{M}(E\lambda)||0\rangle|^2\ , \tag{18}$$

where

$$\langle\nu||\mathcal{M}(E\lambda)||0\rangle = \sum_{ph}\,[X_{ph}^{\nu *}(\lambda) + (-)^{\lambda}Y_{ph}^{\nu *}(\lambda)] \times\langle p||\mathcal{M}(E\lambda)||h\rangle\ , \tag{19}$$

are reduced matrix elements[36] of the electric multipole operators

$$\mathcal{M}(E\lambda;\mu) = \sqrt{\frac{4\pi}{2\lambda+1}}\,er^{\lambda}\mathcal{Y}_{\lambda\mu}(\hat{\mathbf{r}})\ . \tag{20}$$

In Eq. (18) the factor 2 accounts for the spin degeneracy, while the denominator in front of the reduced matrix element results from the fact that the operator $\mathcal{M}(E\lambda)$ has $2\lambda+1$ components. The double bars denote the usual reduced matrix elements, while $\mathcal{Y}_{\lambda\mu}(\hat{\mathbf{r}})$ is a spherical harmonic. In particular, the reduced matrix element $\langle p||\mathcal{M}(E\lambda)||h\rangle$ is given by the expression

$$\langle p||\mathcal{M}(E\lambda)||h\rangle = (-)^{l_p}\sqrt{(2l_p+1)(2l_h+1)}\begin{pmatrix} l_p & \lambda & l_h \\ 0 & 0 & 0\end{pmatrix} \times R(p,h;\lambda)\ , \tag{21}$$

where

$$R(p,h;\lambda) = e\int_0^{\infty} r^{\lambda+2}\mathcal{R}_{n_p,l_p}(r)\mathcal{R}_{n_h,l_h}(r)dr. \tag{22}$$

In the case of a simple two-body force, like the Coulomb interaction, the associated unperturbed particle-hole excitations exhaust the classical energy-weighted sum rule

$$S(E\lambda) = \lambda N_e\frac{\hbar^2e^2}{2m_e}\langle r^{2\lambda-2}\rangle\ , \tag{23}$$

that is

$$\sum_{ph}(\epsilon_{n_p,l_p}-\epsilon_{n_h,l_h})\left|\sqrt{\frac{2}{2\lambda+1}}\,\langle p||\mathcal{M}(E\lambda)||h\rangle\right|^2 = S(E\lambda)\ , \tag{24}$$

where ϵ_{n_i,l_i} are the single-particle energies and the $\langle\,\rangle$ denotes the expectation value over the uncorrelated ground-state density of the cluster as specified by the unperturbed single-particle Hamiltonian H_0.

The result (24) is also valid for the correlated eigenstates and associated eigenvalues E_{ν} of Eq. (5), since the

RPA preserves the energy-weighted sum rule,[31] namely,

$$\sum_{\nu} E_{\nu}\, B(E\lambda, 0 \rightarrow \nu) = S(E\lambda)\ . \tag{25}$$

C. The photoabsorption cross section

Since the incident light has a wavelength much larger than the dimensions of the cluster, the associated electromagnetic field excites only the dipole plasmon, and we need consider only the photoabsorption cross section, σ_{N_e}, for $\lambda = 1$.

In this case, the photoabsorption cross section is related to the imaginary part of the dynamic polarizability, $\alpha(\omega)$, of the valence electrons as follows:

$$\sigma_{N_e} = \frac{4\pi\omega}{c}\mathrm{Im}\alpha(\omega)\ . \tag{26}$$

The dynamic polarizability is given by the expression

$$\alpha(\omega) = -\sum_{\nu}\left\{\frac{B(E1, 0 \rightarrow \nu)}{\hbar\omega - E_{\nu} + i\eta} - \frac{B(E1, 0 \rightarrow \nu)}{\hbar\omega + E_{\nu} + i\eta}\right\}\ . \tag{27}$$

Introducing oscillator strengths f_{ν} normalized to unity, namely,

$$f_{\nu} = \frac{E_{\nu}\, B(E1, 0 \rightarrow \nu)}{S(E1)}\ , \tag{28}$$

the cross section is written as

$$\sigma_{N_e} = \frac{2\pi^2 N_e e^2 \hbar}{m_e c}\sum_{\nu} f_{\nu}\, \delta(\hbar\omega - E_{\nu})\ . \tag{29}$$

The sharp spikes produced by the discrete RPA, and expressed by the Dirac δ function in (29), are naturally broadened and acquire a width Γ due to various damping mechanisms.[16,17] Consequently, when comparing to experimental data, the δ functions are replaced with Lorentzian shapes $L(E_{\nu}, \Gamma_{\nu})$, having a width Γ_{ν} and a maximum at E_{ν} (sometimes also Gaussian shapes may be used). After calculating the constant in front of the sum, the final expression for the photoabsorption cross section per valence electron is given by

$$\sigma = 1.0975\ (\mathrm{eV\,\AA}^2)\ \sum_{\nu} f_{\nu}\, L(E_{\nu}, \Gamma_{\nu})\ . \tag{30}$$

The area under the photoabsorption curve is conserved, namely the contribution of each delocalized electron is

$$\int_0^{\infty} \sigma\, dE = \frac{2\pi^2 e^2 \hbar}{m_e c} = 1.0975\ \ \mathrm{eV\,\AA}^2\ , \tag{31}$$

a property that is essential for the interpretation of the experimental results.

D. Static polarizabilities

The static polarizability α in the RPA is related to the inverse energy-weighted sum $S_{-1}(E1)$. This can be seen from Eq. (27), namely,

$$\alpha = 2\sum_{\nu}\frac{B(E1, 0 \rightarrow \nu)}{E_{\nu}} \ = \ 2S_{-1}(E1)\ . \tag{32}$$

This quantity is to be compared with the classical value of a metal sphere, $\alpha_{\mathrm{cl}} = R^3 = r_s^3 N_e$.

III. RPA RESULTS FOR SODIUM

Figures 2 and 3 display the RPA oscillator strengths per atom for the set of spherical sodium clusters Na_8, Na_{20}, Na_{40}, Na_{58}, Na_{92}, Na_{138}, Na_{196}, Na_{254}, and Na_{338}. They correspond to shell closures of the $1p$, $2s$, $2p$, $1g$, $3s$, $3p$, $3d$, $2h$, and $4p$ orbitals, respectively. The RPA oscillator strengths for Na_8, Na_{20}, and Na_{40} have been discussed in earlier publications,[20,21] where a confrontation against the available experimental observation[4,5,8] was also presented. It was concluded that—apart from a moderate blueshift in the positions—the RPA cross sections accounted fairly well, not only for the main trends, but also for the details of both the location and the profiles of the photoabsorption spectra.

A. Evolution of the interaction between surface-plasmon and *unperturbed* particle-hole transitions

As discussed in Ref. 21 for the case of the smallest Na_8, Na_{20}, and Na_{40} clusters, a prominent result of the matrix RPA calculations was that the surface plasmon may be strongly fragmented. The extent of fragmentation of the surface plasmon depends upon the existence of unperturbed particle-hole transitions that lie close to the original (before the breakup) plasmon. Reference 21 offered a detailed analysis of the fragmentation process by utilizing

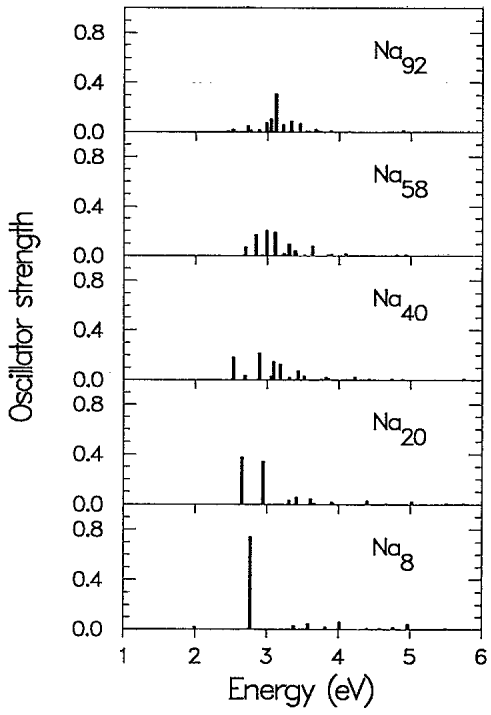

FIG. 2. RPA oscillator strengths per atom for Na_8, Na_{20}, Na_{40}, Na_{58}, and Na_{92} (see the text for a full description).

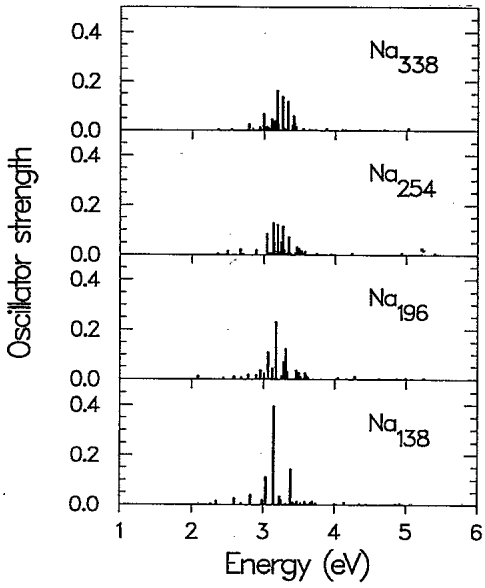

FIG. 3. RPA oscillator strengths per atom for Na_{138}, Na_{196}, Na_{254}, and Na_{338} (see the text for a full description).

restricted subspaces, in addition to the full particle-hole space. An immediate visualization of this process, however, can be achieved by an inspection of Figs. 4 and 5. In fact, Figs. 4 and 5 display the unperturbed oscillator strengths, namely the strength distribution before the RPA linear superposition upon the particle-hole basis is implemented through the diagonalization of the matrix equation (5). The empty arrow denotes the position of the original unbroken surface plasmon. It is apparent that the surface plasmon, in the case of Na_8, falls well within an area empty of particle-hole transitions. As a result, for Na_8, the plasmon does not couple strongly to the unperturbed particle-hole transitions and the extent of fragmentation is small, the photoabsorption profile retaining the shape of one dominant peak.[37]

As seen from Figs. 4 and 5, the particle-hole transitions are organized into two groups, a lower-energy group and a second one at higher energies, having an energy gap between them. The lower-energy group consists exclusively of particle-hole transitions of $\Delta\mathcal{N} = 1$ character, $\mathcal{N} = 2(n-1)+l$ being the single-particle principal quantum number (n is the number of nodes plus one and l is the single-particle angular momentum). The second group consists of all the remaining particle-hole transitions of $\Delta\mathcal{N} \geq 3$ character, with the $\Delta\mathcal{N} = 3$ transitions lying at the edge of the energy gap.

The existence of the energy gap is a consequence of

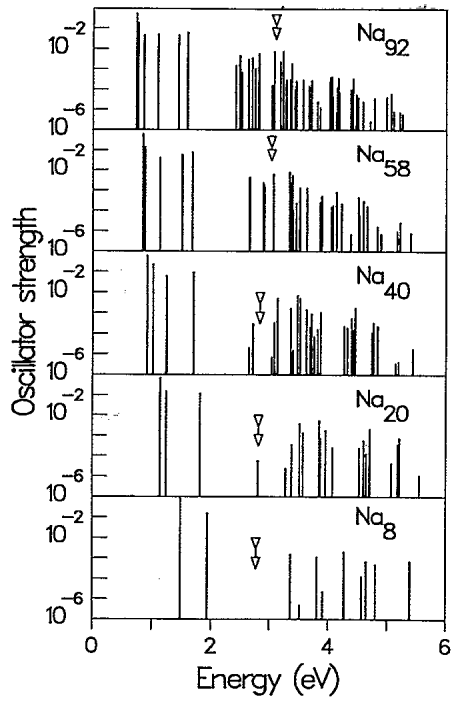

FIG. 4. Unperturbed oscillator strengths per atom for Na_8, Na_{20}, Na_{40}, Na_{58}, and Na_{92}. The scale for the oscillator strength is logarithmic. The empty arrow denotes the position of the surface plasmon. The energy gap between the *low*-energy $\Delta\mathcal{N} = 1$ and the higher-energy $\Delta\mathcal{N} \geq 3$ particle-hole transitions is clearly seen. It becomes smaller with increasing size.

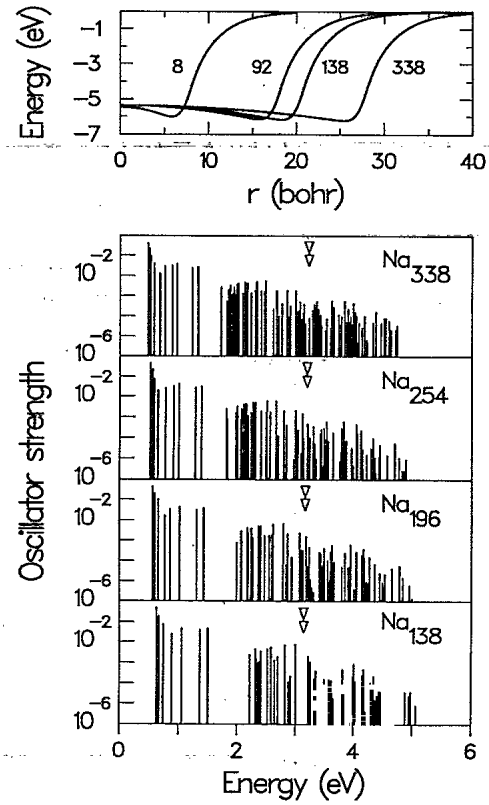

FIG. 5. Unperturbed oscillator strengths per atom for Na_{138}, Na_{196}, Na_{254}, and Na_{338}. The scale for the oscillator strength is logarithmic. The empty arrow denotes the position of the surface plasmon. The energy gap between the low-energy $\Delta\mathcal{N} = 1$ and the higher-energy $\Delta\mathcal{N} \geq 3$ particle-hole transitions is clearly seen. It becomes smaller with increasing size. Top panel: Variations of the effective potentials that bind the delocalized valence electrons as a function of size.

the finite size of the cluster. Indeed, for the ideal case of a harmonic oscillator, all particle-hole transitions with a given $\Delta\mathcal{N}$ are degenerate forming specific shells with a constant energy gap between them. In the case of neutral clusters, only the first gap between the $\Delta\mathcal{N} = 1$ and the $\Delta\mathcal{N} = 3$ transitions survives, since at higher energies the cluster potential flattens, unlike the harmonic-oscillator potential. This flattening of the potential results in the overlap of the $\Delta\mathcal{N} \geq 3$ transitions. The extent of this overlap depends on the size of the cluster, being strongest for the larger clusters. For clusters above Na_{58}, the $\Delta\mathcal{N} \geq 3$ transitions can properly be described as forming a forest of excitations.

Figures 4 and 5 also show that the energy gap diminishes with increasing size. This is a consequence of the increase in the volume of the cluster and of the related fact that the major shell of the spatially equivalent oscillator decreases with increasing size. The behavior of the fragmentation of the plasmon can be grasped by observing that the position of the unbroken surface plasmon (empty arrow) remains almost constant with the size. This is a consequence of the long-range character of the Coulomb force that supplies the energy for the plasmon vibration. The extent of the fragmentation of the photoabsorption strength depends on the relative position of the surface plasmon with respect to the energy gap and the forest of higher-energy excitations. In the case of Na_8, the gap is large and the surface plasmon falls well within the gap away from the higher-energy excitations. Then gradually, the gap diminishes with size, and the surface plasmon first grazes the edge of the gap (cases of Na_{20} and Na_{40}, which exhibit a double-line and a flat multipeak absorption profile, respectively) and then moves slowly, well inside the forest of higher-energy particle-hole excitations. In this respect, the number of actual strength fragments in the RPA response increases, since the number of particle-hole excitations degenerate with the plasmon naturally increases with the size.

However, the distance between any two adjacent strength fragments in the RPA response actually diminishes. As a result, above Na_{58}, the width of the cross section decreases with increasing cluster size, a trend that is opposite to the trend from Na_8 to Na_{40}. In fact, the repulsion between the RPA strength fragments is strongest in the size range of Na_{20} and Na_{40}, and then gradually decreases. The reason is that this repulsion depends upon the coupling between the plasmon and the degenerate particle-hole transitions (for example, in the case of Na_{20}, Ref. 21 has shown that the two members of the double line cannot come closer in energy than $2v$, where v is the effective coupling between the plasmon and the special $2s \rightarrow 3p$ transition). In its turn, this effective coupling depends upon the $\Delta\mathcal{N}$ character of the degenerate particle-hole transitions, the surface plasmon comprising mainly $\Delta\mathcal{N} = 1$ transitions. In the case of Na_{20} and Na_{40}, the plasmon is degenerate with single-particle transitions of $\Delta\mathcal{N} = 3$ character at the edge of the forest. For larger sizes, the plasmon moves well within the forest and is degenerate with transitions of $\Delta\mathcal{N} \geq 5$ character, transitions that progressively exhibit a weaker coupling to the surface plasmon.

Further insight into the matter discussed in this subsection can be obtained from Figs. 6 and 7, where the forward- and backward-going RPA amplitudes [cf. Eq. (5)] for the lightest and the heaviest of the sodium clusters calculated here are shown. In both cases, namely for Na_8 and Na_{338}, the $\Delta\mathcal{N} = 1$ excitations have some of the largest X components, which are also associated with large Y components, and thus with appreciable ground-state correlations. Because the sign of X' s and Y' s is the same, the associated RPA matrix elements of the dipole operator [cf. Eq. (19)] are quenched. This is a natural consequence of the fact that the residual interaction is repulsive and therefore the RPA centroid of the resonance is higher than the original $\Delta\mathcal{N} = 1$ particle-hole excitations. Because the EWSR is preserved in the RPA, the associated $B(E1, 0 \rightarrow \nu)$ has to decrease compared to the unperturbed case.

In the case of Na_8, the $\Delta\mathcal{N} = 3$ and higher excitations lead to an enhancement of the $B(E1, 0 \rightarrow \nu)$ elements, as the X and Y components in each pair have opposite sign. This antiquenching is natural for transitions lying higher than the resonance, as the energy denominator of the dynamical polarizability [cf. Eq. (27)] changes sign.

The situation is very different in the case of Na_{338}, where very large $\Delta\mathcal{N} \geq 3$ X components, larger than any of the $\Delta\mathcal{N} = 1$ components, are found. These components are, however, not associated with large Y components. In fact, in this case, the large X amplitudes

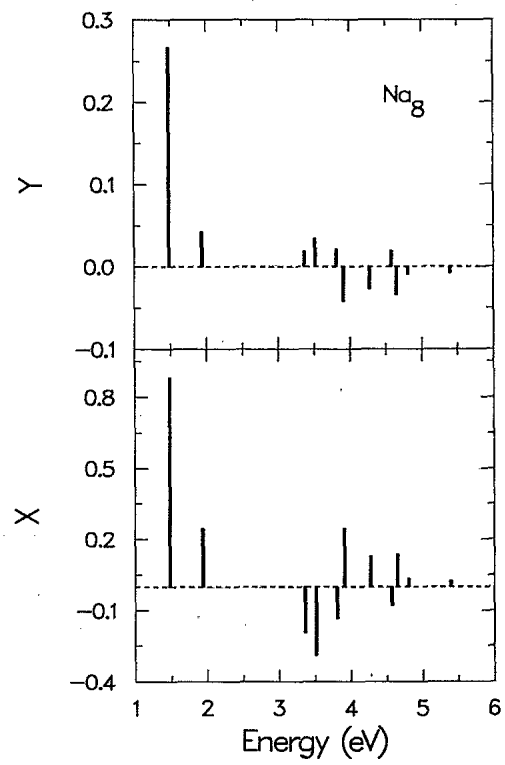

FIG. 6. The forward- and backward-going X and Y RPA amplitudes for Na_8. The choice of phase for the values in the figure is such that all the associated matrix elements, $\langle p||\mathcal{M}(E1)||h\rangle$ [cf. Eq. (19)], of the dipole operator should be positive.

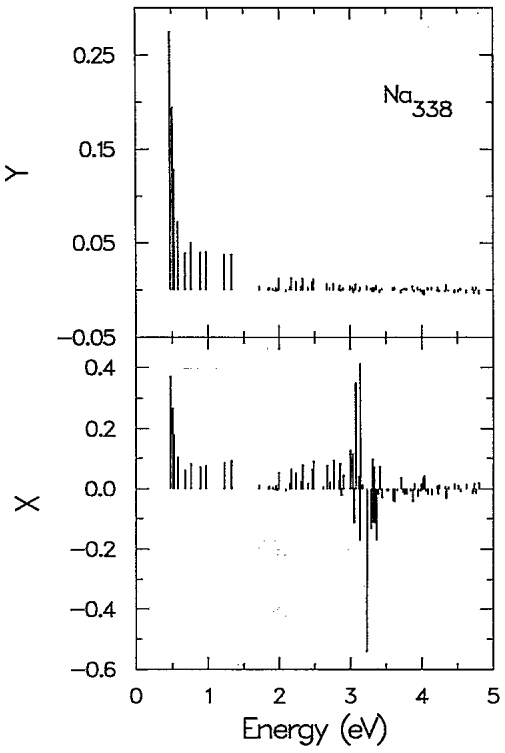

FIG. 7. The forward- and backward-going X and Y RPA amplitudes for Na_{338}. The choice of phase for the values in the figure is such that all the associated matrix elements, $\langle p||\mathcal{M}(E1)||h\rangle$ [cf. Eq. (19)], of the dipole operator should be positive.

result from the accidental degeneracy of the surface plasmon with unspecific particle-hole excitations. This is the phenomenon of Landau damping.

B. RPA cross sections: Evolution of plasmon width and position

Figure 8 and 9 display the cross sections that result from the RPA oscillator strengths after folding them with Lorentzian line shapes. An intrinsic width of 10% was used throughout in this folding. In keeping with the results presented in Refs. 15–19, this intrinsic width is expected to reflect the coupling of the plasmon to thermal fluctuations of the surface. Starting from Na_8 and moving to larger clusters, the cross section first exhibits one dominant peak, then two peaks for Na_{20}, and then, for Na_{40}, a very broad, flat profile encompassing several smaller peaks of comparable strength. The one-peak profile familiar from the classical Mie theory, however, starts reappearing with Na_{58} and persists without interruption up to Na_{338}. For all sizes, the FWHM (full width at half maximum) of the photoabsorption cross section is largest for Na_{40}, and for higher mass numbers, it decreases slowly. This is a consequence of the fact that, for sizes larger than Na_{58}, the repulsion between the RPA strength fragments decreases with size while at the same time the number of fragments increases, as explained earlier. Figure 10 displays the FWHM extracted from the RPA cross sections of Figs. 8 and 9 versus the prediction of the $1/R$ law with the correct proportionality coefficient and frequency dependence determined in Ref. 12

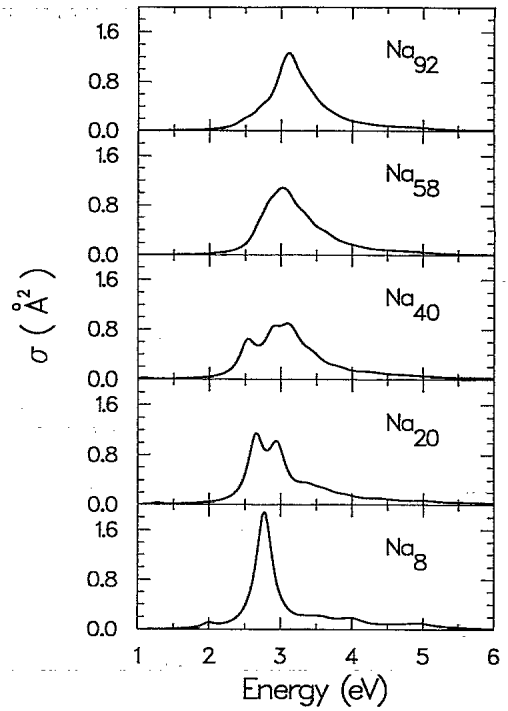

FIG. 8. RPA cross sections per atom for Na_8, Na_{20}, Na_{40}, Na_{58}, and Na_{92}. The curves were produced by folding the corresponding RPA oscillator strengths with Lorentzians according to Eq. (30). For the Lorentzians a 10% intrinsic width was used throughout.

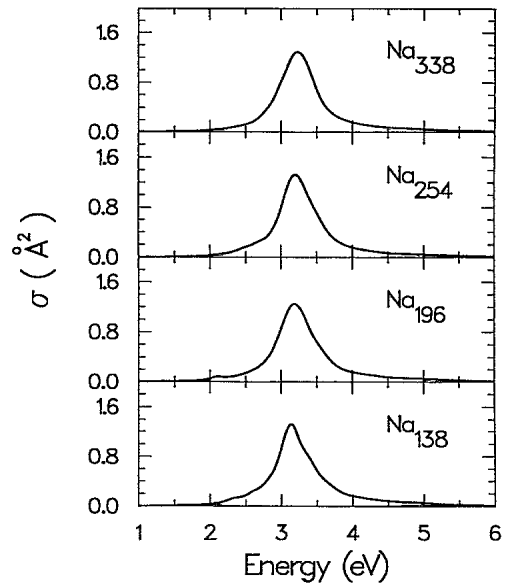

FIG. 9. RPA cross sections per atom for Na_{138}, Na_{196}, Na_{254}, and Na_{338}. The curves were produced by folding the corresponding RPA oscillator strengths with Lorentzians according to Eq. (30). For the Lorentzians a 10% intrinsic width was used throughout.

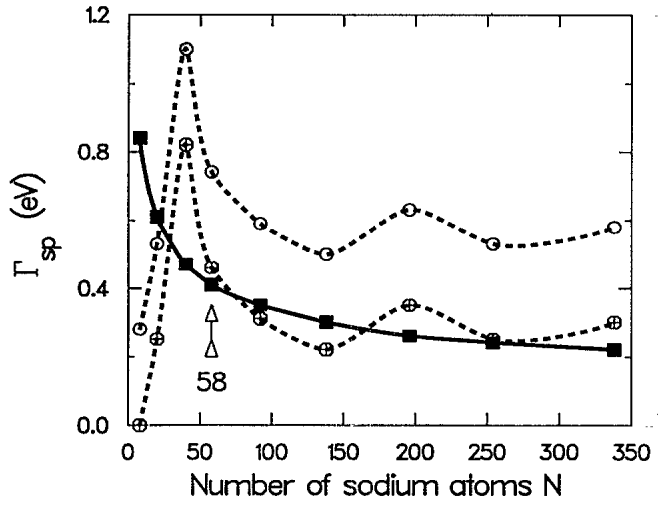

FIG. 10. The width of the surface plasmon Γ_{sp} vs the number of sodium atoms N. Upper dashed curve: The FWHM extracted from the RPA cross sections in Figs. 8 and 9. The open circles correspond to the mass numbers displayed in these two figures. Lower dashed curve: The upper dashed curve shifted so that the FWHM of Na_8 is zero. In this way, the 10% intrinsic width that was used to smooth the RPA response has been uniformly subtracted, and the lower dashed curve represents exclusively the contribution of Landau damping. Solid curve: The predicted width according to the $1/R$ law. The correct proportionality coefficient of Ref. 12 has been used. The solid squares correspond to the mass numbers calculated in the present work, namely 8, 20, 40, 58, 92, 138, 196, 254, and 338. From an inspection of the figure, it can be concluded that the $1/R$ law is approximately valid for masses as low as Na_{58}. Below Na_{58}, however, it breaks down, as exemplified by the sudden rise and subsequent rapid fall of the dashed curves.

[see, in particular, Eqs. (61)–(63)]. Since the FWHM from Figs. 8 and 9 reflects also the thermal broadening that was taken here to be a uniform 10%, the corresponding curve (upper dashed curve in Fig. 10) was corrected by subtracting throughout a component of 0.28 eV. The remaining width (lower dashed curve) is due exclusively now to Landau damping, and Na_8 properly exhibits zero Landau damping. Apart from some reasonable oscillations due to residual shell structure of the particle-hole subspace, the renormalized curve agrees fairly well on the average with the $1/R$ law for sizes equal or larger than Na_{58}. However, in the size range from Na_8 to Na_{40}, the $1/R$ law breaks down. The breakdown of the $1/R$ law for the small sizes in the case of sodium and potassium clusters was noticed in earlier publications[4,6,12] and is clearly illustrated in Fig. 10 by the sudden drop in the dashed curves. The exact point, however, where this drop appears may be dependent upon the electronic density, and, in the case of metals with electronic densities much higher than sodium and potassium, it may well be pushed below the number of 40 electrons. This conjecture appears to explain the recent experimental observations on small Hg clusters,[38] where the $1/R$ law was found valid down to Hg_{10}^+ (19 electrons). Probably, in this case, the FWHM follows a curve like the upper dashed curve in Fig. 10, namely, the proportionality coefficient for the $1/R$ law is augmented due to thermal fluctuations of the mean field.

A second important feature revealed by Figs. 8 and 9 is the evolution of the position of the plasmon (in the case of Na_{20} and Na_{40}, the position of the plasmon is taken as the average of the photoabsorption curve; in all other cases, the position is taken as the top of the single peak). Indeed, this position starts as low as 2.8 eV for Na_8, but very rapidly moves higher at 3.25 eV for Na_{338} in agreement with the Mie prediction (3.4 eV) for a classical metal sphere with the electronic density of the bulk sodium.

That the position of the resonance approaches the bulk value in the limit of large mass numbers has been earlier anticipated from simplified RPA approaches that overlook the detailed particle-hole structure.[34,39,40] It results from the diminishing importance with size of both the electronic spill-out and the exchange-correlation contribution to the residual interaction. As Fig. 11 shows, the energy of the photoresonance calculated in the matrix RPA increases very rapidly and is very close to the classical value already in the mass area between 100 to 150 sodium atoms. This rapid approach to the classical limit has also been seen experimentally[27] in the reflectivity spectra of small isolated sodium clusters adsorbed on a boron nitride surface. The RPA results and the experimental observations are plotted in Fig. 11.

Ekardt[22] has calculated the photoabsorption for the three sizes Na_{20}, Na_{92}, and Na_{198} using the TDLDA approach. His results are consistent with the corresponding matrix RPA results. Beck[24] has calculated in the TDLDA the position of the surface plasmon for sodium clusters from 8 to 198 atoms. However, this latter calculation exhibits a sharp discontinuous step between the plasmon positions for Na_{58} and Na_{92}, unlike the present result that shows a smooth increase. In the

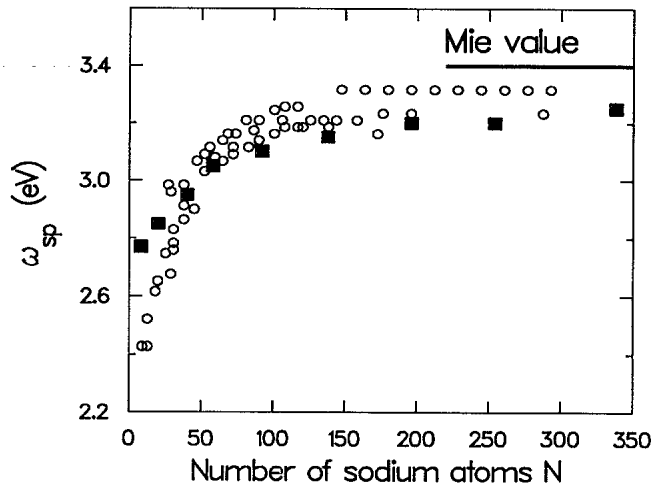

FIG. 11. The energy of the photoresonance in neutral sodium clusters as a function of the number of atoms. Solid squares: Energies extracted from the RPA cross sections in Figs. 8 and 9. Open circles: Experimental results from Ref. 27. The Mie value (Refs. 9 and 4) is also denoted.

mass area from 100 to 200, the same TDLDA calculation has reported[27] positions for the photoresonance at slightly lower energies, namely from 3.0 to 3.1 eV, unlike the present calculation which yielded positions from 3.15 to 3.20 eV in better agreement with the experiment. A Hartree-Fock RPA study[41] of the three clusters Na_{20}, Na_{40}, and Na_{92} has found that the position of the photoresonance remains almost constant with size, and does not approach the classical Mie value, unlike the present LDA-RPA calculation. Since the Hartree-Fock RPA neglects correlation effects, the upward movement of the photoresonance in the LDA-RPA can be attributed primarily to the rapid weakening of the correlation contribution. In fact, the exchange contribution is also weakening with the size of the cluster, but apparently in a much slower pace than the contribution from the correlation.

C. A unified view for the evolution of the photoabsorption

The variations in the distribution of the unperturbed particle-hole transitions exhibited in Figs. 4 and 5 are generated by size changes sustained by the effective potential that binds the delocalized valence electrons. The variation of the potentials with the mass number for the neutral sodium clusters is displayed in the uppermost frame of Fig. 5. These potentials retain a constant depth, but their width keeps increasing following roughly the radius, $R = r_s N^{1/3}$, of the positive jellium background, where for sodium we have used r_s=4.0 a.u. In this respect, one can assign the variations of the photoabsorption with size to a single factor, namely, to the changes of the effective potential.

It should be emphasized here that the LDA-RPA upon a jellium background offers the vehicle for formulating a unified view of the evolution of the photoabsorption profiles as due to variations in the effective mean field. Apart from changes due to the size, the effective jellium potentials can change also due to variations in the total charge of the cluster (positive ions, neutral clusters, or negative ions), as well as in the chemical composition of the cluster (bimetallic clusters). The description of the variations of the optical spectra with the total charge was presented in Refs. 42, 17, and 20. Reference 43 discussed the variations of the optical response induced by an impurity inside an otherwise homonuclear cluster.

As seen from the confrontation of the matrix RPA results against the experimental observation, the agreement between the jellium model and the experiment becomes better with increasing size. This behavior is to be contrasted with the behavior of relative abundances and stabilities for larger sizes. For cold sodium clusters, it has been found that the electronic magic numbers persist up to a size of 1500 to 2000 atoms; for larger sizes, the relative stability is controlled by ionic effects and the magic numbers correspond to geometric atomic packing.[44] In the case of the optical properties, the central potential description and the related classical Mie photoresonance theory are, in principle, valid up to an infinite number of atoms. The explanation for this different behavior between ground-state properties and optical properties lies with the smallness of the single-particle energy gaps around the Fermi energy, as well as of the total-energy differences from one size to the next, compared to the much larger energy of the plasmon. In fact, the energy variations associated with the ground-state quantities become smaller the larger the size, unlike the energy of the plasmon that reaches a constant value.

D. Static polarizabilities

We calculate the static polarizabilities using the RPA expression (32). The results are listed in Table I. For the smaller clusters, the jellium LDA-RPA results are lower than the experimental observation. This behavior agrees with earlier TDLDA calculations,[22,45] and is related to the systematic blueshift found in the position of the photoresonance with respect to the observed location. This discrepancy in the positions, however, between theory and experiment, diminishes very fast with the size as seen from Fig. 11. In analogy, the corresponding discrepancy for the static polarizability should decrease for higher masses, even though a direct comparison is not possible, since experimental values are only available for sodium clusters with less than 40 atoms. One can, however, observe that the RPA values in Table I decrease smoothly with size and approach the classical value of unity. It may appear that the approach of the static polarizabilities to the classical value is slower than the corresponding approach of the plasmon position to the Mie value (cf. Fig. 11). The two trends, however, are in consonance, since the position of the plasmon is related to the static polarizability through the square root, as can be found by combining the Thomas-Reiche-Kuhn and the inverse energy-weighted sum rules, namely,

$$\hbar\omega = \left(\frac{4}{r_s^3}\frac{1}{\alpha}\right)^{1/2} \text{Ry bohr}^{3/2} , \tag{33}$$

where α is given in the dimensionless units of the actual static polarizability over the classical value $R^3 = r_s^3 N_e$.

Of course, for Eq. (33) to be valid, most of the strength

TABLE I. Static polarizabilities α_{RPA} for sodium clusters calculated in the matrix RPA-LDA compared to measured experimental values. The static polarizabilities are in units of the value for the classical sphere, $\alpha_{\text{cl}} = R^3 = r_s^3 N$.

Mass number N	α_{RPA}	Experimental polarizability[a]
8	1.34	1.72
20	1.33	1.62
40	1.29	1.57
58	1.19	
92	1.17	
138	1.15	
196	1.15	
254	1.12	
338	1.12	
1982	1.04	

[a]From Ref. 4.

must be concentrated in a narrow-energy region. For Na_{338}, Table I lists $\alpha = 1.12$, and Eq. (33) yields $\hbar\omega$=3.21 eV in very good agreement with the value 3.25 eV extracted from the maximum in the cross-section profile displayed in Fig. 9.

The 20% discrepancy between experiment and RPA-LDA in the case of the smaller sodium clusters ($N_e \leq 40$) has motivated several attempts to improve the description of the electronic gas beyond the LDA. To this end empirical self-interaction corrections (SIC) have been introduced.[46–48] In general, the SIC results for the static polarizabilities move in the right direction toward the experimental values. Reference 41 has carried out a consistent Hartree-Fock-RPA calculation upon a jellium background. In the Hartree-Fock approximation, the spurious self-interaction is canceled fully by the exchange terms, but still it was found that not sufficient improvement with the experiment was achieved.

Another venue for overcoming this discrepancy starts from the view that it is due to the neglecting of the ionic structure.[49] Apart from an improvement in the static polarizabilities and in the position of the plasmon, this venue accounts for several crucial additional features in the photoabsorption profiles, e.g., for Na_8 the smaller satellite peak at low energies is properly placed at 2.0 eV (for the experimental evidence, cf. the work of Pollack and co-workers, Ref. 8). In contrast, the SIC-TDLDA (Refs. 47 and 48) fails to position this satellite peak at the right energy. The satellite peak is even more prominent in the case of Cs_8,[7] and again has been explained as an effect of the ionic structure in Ref. 49. SIC-TDLDA calculations for Cs_8 are not as yet available.

IV. THE CASE OF LARGE POTASSIUM CLUSTERS

Figure 12 displays the matrix RPA oscillator strengths for the case of the large potassium clusters K_{484}, K^+_{485}, K_{940}, and K^+_{941}. The behavior of the response is quite analogous to that found for the large sodium clusters, namely the strength fragments bunch densely around 2.45 to 2.5 eV falling within a small energy range of approximately 0.20 eV. In other words, the classical Mie value for potassium [2.54 eV according to formula (1) for r_s=4.86 a.u.] has firmly been reached at these sizes, and the response will exhibit a single-peak profile after the folding with appropriate Lorentzians.

One can also see that there is no difference in practice between the neutral and the singly charged species. Indeed, the influence of the total charge $N_z e$ depends upon the ratio N_z/N_e of the total charge versus the total number of delocalized electrons, this ratio being very small for the large sizes considered here.

Unlike the case of sodium, however, recent experimental results by Bréchignac and collaborators[28] disagree with the jellium LDA-RPA prediction concerning the position of the plasmon in large potassium clusters. Specifically, Bréchignac *et al.* have found the plasmon energy at approximately 2.05 eV, substantially lower than the classical Mie value calculated from Eq. (1).

It appears that the electrons in potassium should be assigned an effective mass $m_{\rm eff}$ larger than the free-electron mass m_e used throughout in the RPA calculations. In this case, the Thomas-Reiche-Kuhn sum rule modifies as follows:

$$S(E1) = N_e \frac{\hbar^2 e^2}{2\, m_{\rm eff}} \tag{34}$$

and the position of the photoresonance can be lowered for $f_{\rm eff} = m_{\rm eff}/m_e > 1$. Taking into consideration the effective mass, the Mie-plasmon position for a sphere is modified as

$$\hbar\omega_{\rm Mie,mod} = \left(\frac{4}{r_s^3\, f_{\rm eff}}\right)^{1/2} \text{Ry bohr}^{3/2} . \tag{35}$$

It is has been found that neither the volume plasmon nor the plane-surface plasmon in potassium has the value predicted by the plasmon formula (2) with the free-electron mass. These values are, respectively, 4.4 eV and $4.4/\sqrt{2}$=3.11 eV. However, the corresponding experimental values are redshifted at 3.81 (Ref. 50) and 2.74 eV,[51] respectively. Use of an effective mass $f_{\rm eff} = 1.3$ can account for this redshift for both the volume and the plane-surface case, as can be seen from $\hbar\omega_{\rm Mie,mod}\sqrt{3}$ and $\hbar\omega_{\rm Mie,mod}\sqrt{3/2}$. For the case of the sphere, Eq. (35) yields, for $f_{\rm eff} = 1.3$, the value of 2.23 eV as the limiting value for large potassium clusters.

Motivated from this behavior of the volume and plane-

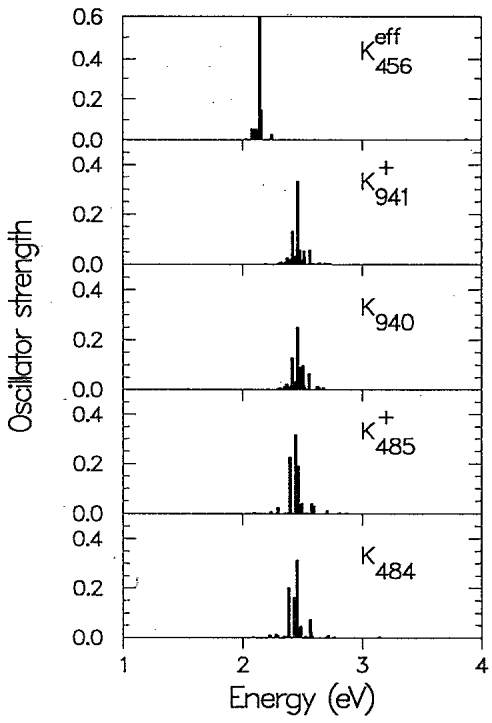

FIG. 12. RPA oscillator strengths per atom for the neutral K_{484} and K_{940}, compared to the singly charged K^+_{485} and K^+_{941}. They have been calculated using free-electron-gas parameters. Top panel: RPA oscillator strength per atom for the neutral K_{456}, but calculated using an effective electron mass $m_{\rm eff}/m_e = 1.3$.

surface plasmon, we modified the jellium code for the effective potentials and the matrix RPA code to accept an effective mass as an input, and we carried out a full RPA calculation for K_{456} (Ref. 52) using the same value $f_{\text{eff}} = 1.3$. From Fig. 12 it can be seen that the strength fragments bunch now around 2.15 eV in good agreement with the experimental value[28] and in consonance with the limiting value of 2.23 eV found from the modified Mie expression (35).

The use of $f_{\text{eff}} = 1.3$ for potassium should be taken with a certain caution, since, from the bulk, it is known that core-polarization contributions can have similar effects as the effective mass for the electrons. We do not wish to go into details on this subject, and we restrict ourselves here to point out that the LDA-RPA converges to the classical Mie value only when the free-electron mass has been input. Consideration of an effective mass or of core-polarization contributions, deduced from the bulk case, will modify the large-particle RPA limit, and may eventually bring the theory in agreement with the experiment in the case of potassium clusters.

V. SUMMARY AND CONCLUSION

The matrix RPA-LDA upon a uniform jellium background is able to describe rather accurately the observed approach towards the bulk of the optical properties of spherical neutral sodium microclusters. The moderate discrepancies observed between the theoretical predictions and the experimental data, concerning the centroid of the strength functions and the static polarizabilities in the case of small ($N_e \leq 40$) mass-number clusters, diminish rapidly with size. Concerning the photoabsorption profiles, theory provides an overall account of the experimental data.[20,21]

The present theory predicts two regimes for the optical properties of alkali-metal clusters. The first applies to the smaller-size clusters and is characterized by response functions displaying extremely variable and highly individualistic quantum-size effects eventually leading to multipeak fragmentation of the total strength. The second regime applies to the larger sizes and is characterized by a smooth response exhibiting a single peak and a width following the $1/R$ law. The transition between the two regimes happens around Na_{58}.

The large-limit RPA parameters for sodium characterizing the surface plasmon are $\omega_{\text{sp}} \approx 3.4$ eV (centroid) and $\Gamma \approx 1.5N^{-1/3}$ eV (FWHM due to Landau damping). The results of the RPA calculations show a rapid variation of the corresponding quantities towards these values within the lightest 10^2-particle clusters. In fact, Na_{138} displays a collective plasmon excitation characterized by $\omega_{\text{sp}} \approx 3.15$ eV and $\Gamma \approx 1.2N^{-1/3}$ eV. That is, the energy centroid reaches a plateau which differs from the Mie value by approximately 7% already for $N = 138$, while the predicted value of Γ oscillates around the $1/R$ law displaying 25% fluctuations. These results are rather unexpected, in view of the fact that the average distance between the single-particle orbitals belonging to different major shells is $\hbar\omega_0 \approx \epsilon_F N^{-1/3}$ eV ≈ 0.6 eV ($N = 138$), much larger than the typical cluster temperatures.

While for sodium clusters the centroid of the photoresonance comes close to the Mie value of the free-electron gas already for clusters containing a few hundred atoms, the situation is quite different for potassium clusters. In this case, experimental evidence exists[28] that the corresponding limiting value is modified by effective-mass and core-polarization effects, in a way consistent with the behavior of the volume and plane-surface plasmons in the bulk.[53] The use of bulk effective parameters can bring the RPA predictions for large potassium clusters in agreement with the experiment.

In conclusion, the matrix RPA-LDA approach provides a simple, yet accurate, picture of the evolution of the optical properties of metal clusters, the unifying element being the average potential describing the single-particle motion. Thus the changes in the photoabsorption cross sections can be related to changes in the effective potentials resulting from variations in the size (present work and Refs. 21 and 12), or from variations in the total charge,[42,20,17] or even from the presence of impurities.[43,49]

ACKNOWLEDGMENTS

We wish to thank C. Bréchignac and H. Haberland for sending us experimental information prior to publication.

*Present address: School of Physics, Georgia Institute of Technology, Atlanta, GA 30332-0430.

[1] W.A. de Heer, W.D. Knight, M.Y. Chou, and M.L. Cohen, in *Solid State Physics*, edited by H. Ehrenreich, F. Seitz, and D. Turnbull (Academic, New York, 1987), Vol. 40, p. 93.

[2] U. Kreibig and L. Genzel, Surf. Sci. **156**, 678 (1985), and references therein.

[3] W.A. de Heer *et al.*, Phys. Rev. Lett. **59**, 1805 (1987).

[4] K. Selby, M. Vollmer, J. Masui, V. Kresin, W.A. de Heer, and W.D. Knight, Phys. Rev. B **40**, 5417 (1989).

[5] K. Selby, V. Kresin, J. Masui, M. Vollmer, W.A. de Heer, A. Scheidemann, and W.D. Knight, Phys. Rev. B **43**, 4565 (1991); K. Selby, Ph.D. thesis, University of California, Berkeley, 1990.

[6] C. Bréchignac, Ph. Cahuzac, F. Carlier, and J. Leygnier, Chem. Phys. Lett. **164**, 433 (1989).

[7] H. Fallgren and T.P. Martin, Chem. Phys. Lett. **168**, 233 (1990).

[8] S. Pollack, C.R.C. Wang, and M.M. Kappes, J. Chem. Phys. **94**, 2496 (1991); C.R.C. Wang, S. Pollack, and M.M. Kappes, Chem. Phys. Lett. **166**, 26 (1990); C.R.C. Wang, S. Pollack, D. Cameron, and M.M. Kappes, J. Chem. Phys. **93**, 3787 (1990).

[9] G. Mie, Ann. Phys. (Leipzig) **25**, 377 (1908).

[10] A. Kawabata and R. Kubo, J. Phys. Soc. Jpn. **21**, 1765 (1966).

[11] A.A. Lushnikov and A.J. Simonov, Z. Phys. **270**, 17 (1974).

[12] C. Yannouleas and R.A. Broglia, Ann. Phys. (N.Y.) **217**, 105 (1992).

[13]In exploring the analogies between cluster physics and nuclear physics, it is interesting to note that a $1/R$ dependence for the widths of nuclear giant resonances has been proposed within the framework of one-body, wall dissipation [J. Blocki, Y. Boneh, J.R. Nix, J. Randrup, M. Robel, A.J. Sierk, and W.J. Swiatecki, Ann. Phys. (N.Y.) **113**, 330 (1978); C. Yannouleas, Nucl. Phys. A **439**, 336 (1985)].
[14]L.D. Landau, J. Phys. USSR **10**, 25 (1946).
[15]G.F. Bertsch and D. Tománek, Phys. Rev. B **40**, 2749 (1989).
[16]J.M. Pacheco and R.A. Broglia, Phys. Rev. Lett. **62**, 1400 (1989).
[17]C. Yannouleas, J.M. Pacheco, and R.A. Broglia, Phys. Rev. B **41**, 6088 (1990).
[18]J.M. Pacheco, R.A. Broglia, and B.R. Mottelson, Z. Phys. D **21**, 289 (1991).
[19]Z. Penzar, W. Ekardt, and A. Rubio, Phys. Rev. B **42**, 5040 (1990).
[20]C. Yannouleas, R.A. Broglia, M. Brack, and P.F. Bortignon, Phys. Rev. Lett. **63**, 255 (1989).
[21]C. Yannouleas and R.A. Broglia, Phys. Rev. A **44**, 5793 (1991).
[22]W. Ekardt, Phys. Rev. B **31**, 6360 (1985).
[23]W. Ekardt and Z. Penzar, Phys. Rev. B **43**, 1322 (1991).
[24]D.E. Beck, Phys. Rev. B **35**, 7325 (1987).
[25]D.E. Beck, Phys. Rev. B **43**, 7301 (1991).
[26]The optical response of very small sodium clusters ($\leq$ 8 atoms) has been successfully described with *ab initio* configuration-interaction chemical methods (Ref. 29). These methods, however, have failed to describe the double line in Na_{20} as measured by Pollack and co-workers (Ref. 8). A double line, in agreement with the RPA prediction, has also very recently been observed in Ag_{20} [S. Fedrigo, W. Harbich, and J. Buttet (unpublished)]. *Ab initio* calculations for the photoabsorption of Na_{40} are not available at present.
[27]J.H. Parks and S.A. McDonald, Phys. Rev. Lett. **62**, 2301 (1989).
[28]C. Bréchignac, Ph. Cahuzac, N. Kebaili, J. Leygnier, and A. Sarfati, Phys. Rev. Lett. **68**, 3916 (1992).
[29]V. Bonačić-Koutecký, P. Fantucci, and J. Koutecký, Chem. Rev. **91**, 1035 (1991); J. Chem. Phys. **93**, 3802 (1990).
[30]The *RPA Program for Jellium Spheres* [G. Bertsch, Comput. Phys. Commun. **60**, 247 (1990)] [sometimes also referred to as JELLYRPA (Ref. 8)] calculates the linear response using the polarization propagator method in the coordinate space. Thus, it is similar to the TDLDA treatment, unlike the matrix RPA formalism, which uses a matrix diagonalization approach in the particle-hole space.
[31]D.J. Rowe, *Nuclear Collective Motion* (Methuen, London, 1970), Chaps. 4, 16, and 14.
[32]G.E. Brown, L. Castillejo, and J.A. Evans, Nucl. Phys. **22**, 1 (1961).
[33]A.R. Edmonds, *Angular Momentum in Quantum Physics* (University Press, Princeton, 1974).
[34]M. Brack, Phys. Rev. B **39**, 3533 (1989).
[35]O. Gunnarsson and B.I. Lundqvist, Phys. Rev. B **13**, 4274 (1976).
[36]A. Bohr and B.R. Mottelson, *Nuclear Structure* (Benjamin, Reading, MA, 1969), Vol. I, Sec. 1A-5.
[37]In addition to the dominant peak at 2.52 eV, the observed photoabsorption of Na_8 exhibits several weaker but important features, namely, a small peak at the low energy of 2.0 eV and a high-energy tail. The matrix RPA upon a jellium background describes sufficiently well this additional structure (cf. Refs. 20 and 21). Improvement between theory and experiment is achieved by considering modified-jellium effects, as described in Ref. 49. In the present paper, however, we concentrate on the dominant features, since we are interested in describing the overall evolution of the photoabsorption with size. The smaller satellite peak at lower energy, predicted by the matrix RPA for pure clusters with eight delocalized electrons, has also been observed in Cs_8 (Ref. 7), and very recently in the case of Ag_8 [W. Harbich, S. Fedrigo, and J. Buttet, Chem. Phys. Lett. **195**, 613 (1992)].
[38]H. Haberland, B. von Issendorff, Ji Yufeng, and Th. Kolar, Phys. Rev. Lett. **69**, 3212 (1992).
[39]Ll. Serra, F. Garcias, M. Barranco, J. Navarro, C. Balbás, and A. Mañanes, Phys. Rev. B **39**, 8247 (1989).
[40]V. Kresin, Phys. Rev. B **39**, 3042 (1989); **40**, 12 507 (1989).
[41]C. Guet and W.R. Johnson, Phys. Rev. B **45**, 11 283 (1992)
[42]C. Yannouleas, Chem. Phys. Lett. **193**, 587 (1992).
[43]C. Yannouleas, P. Jena, and S.N. Khanna, Phys. Rev. B **46**, 9751 (1992).
[44]T.P. Martin, T. Bergmann, H. Göhlich, and T. Lange, Chem. Phys. Lett. **172**, 209 (1990).
[45]D.E. Beck, Phys. Rev. B **30**, 6935 (1984).
[46]P. Stampfli and K.H. Benemann, Phys. Rev. B **39**, 1007 (1989).
[47]S. Saito, G.F. Bertsch, and D. Tománek, Phys. Rev. B **43**, 6804 (1991).
[48]J.M. Pacheco and W. Ekardt, Z. Phys. D **24**, 65 (1992).
[49]C. Yannouleas and R.A. Broglia, Europhys. Lett. **15**, 843 (1991).
[50]A. vom Felde, J. Spröser-Prou, and J. Fink, Phys. Rev. B **40**, 10 181 (1989).
[51]K.D. Tsuei, E.W. Plummer, and P.J. Feibelman, Phys. Rev. Lett. **63**, 2256 (1989).
[52]Because the use of the effective mass has influenced the effective binding potential, 484 electrons do not close a shell as in the case of the free-electron mass. For $f_{\text{eff}} = 1.3$, however, a shell closure takes place at 456 electrons. Since the slow-variation plateau has already been reached, the small difference in the number of electrons does not influence the position of the plasmon.
[53]In particular, in the case of Na, K, Rb, and Cs, the experimental bulk volume plasmon is lower than the corresponding Drude value by 5%, 13%, 14%, and 18% (Ref. 50), respectively. These alkali metals behave as nearly-free-electron metals, but only sodium is closest to the ideal case of a free-electron gas. The experimental results on the surface plasmon in large potassium and sodium clusters are in close agreement with this behavior in the bulk. For lithium, Rasigni and Rasigni [J. Opt. Soc. Am. **67**, 54 (1977)] have found for the bulk plasmon a value of 6.73 eV, which is 16% below the Drude value. A Kramers-Kronig analysis in terms of a nearly-free-electron model ascribes this discrepancy to an effective mass of $m_{\text{eff}} = 1.80 m_e$. Recent optical measurements on large lithium clusters [C. Bréchignac *et al.* (unpublished)] find a behavior in close analogy again with the bulk.